Biochimica et Biophysica Acta 1804 (2010) 115–123

Contents lists available at ScienceDirect

Biochimica et Biophysica Acta

journal homepage: www.elsevier.com/locate/bbapap

A new topology of ACBP from *Moniliophthora perniciosa*

Paulo S. Monzani [a], Humberto M. Pereira [b], Fernando A. Melo [b], Flávio V. Meirelles [c], Glaucius Oliva [b], Júlio C.M. Cascardo [a,*]

[a] Departamento de Ciências Biológicas, Laboratório de Proteômica, Centro de Biotecnologia e Genética, Universidade Estadual de Santa Cruz, Ilhéus, BA, CEP 45662-900, Brazil
[b] Instituto de Física de São Carlos, Universidade de São Paulo, São Carlos, SP, Brazil
[c] Departamento de Ciências Básicas, Faculdade de Zootecnia e Engenharia de Alimentos, Universidade de São Paulo, Pirassununga, SP, Brazil

ARTICLE INFO

Article history:
Received 23 April 2009
Received in revised form 11 September 2009
Accepted 16 September 2009
Available online 24 September 2009

Keywords:
ACBP
Characterization
Crystal structure
Four-helix bundle
Moniliophthora perniciosa and Witches' broom disease

ABSTRACT

Acyl-CoA binding protein (ACBP) is a housekeeping protein and is an essential protein in human cell lines and in *Trypanosoma brucei*. The ACBP of *Moniliophthora perniciosa* is composed of 104 amino acids and is possibly a non-classic isoform exclusively from Basidiomycetes. The *M. perniciosa acbp* gene was cloned, and the protein was expressed and purified. Acyl-CoA ester binding was analyzed by isoelectric focusing, native gel electrophoresis and isothermal titration calorimetry. Our results suggest an increasing affinity of ACBP for longer acyl-CoA esters, such as myristoyl-CoA to arachidoyl-CoA, and best fit modeling indicates two binding sites. ACBP undergoes a shift from a monomeric to a dimeric state, as shown by dynamic light scattering, fluorescence anisotropy and native gel electrophoresis in the absence and presence of the ligand. The protein's structure was determined at 1.6 Å resolution and revealed a new topology for ACBP, containing five α-helices instead of four. α-helices 1, 2, 3 and 4 adopted a bundled arrangement that is unique from the previously determined four-helix folds of ACBP, while α-helices 1, 2, 4 and 5 formed a classical four-helix bundle. A MES molecule was found in the CoA binding site, suggesting that the CoA site could be a target for small compound screening.

1. Introduction

The basidiomycete *Moniliophthora perniciosa* is the causal agent of witches' broom disease in the cacao plant and is considered to be the main phytopathogen of the cacao plant, causing a marked decrease in cacao production. Commercial fungicides cannot feasibly be used to control this infection [1]; therefore, efforts to find new drug targets for controlling this plague and methods for producing more resistant plants are of great importance.

Acyl-CoA binding protein (ACBP) is a widely distributed and highly conserved cytosolic protein whose molecular mass is approximately 10 kDa. ACBP has been found in all tested eukaryotes and is expressed in most cells and tissues [2]. ACBP binds long chain acyl-CoA esters (C_{12}–C_{22}) with high specificity and affinity (K_d, 1–10 nM) [3], and *in vitro*/*vivo* experiments suggest that ACBP acts as an intracellular acyl-CoA transporter and contributes to the formation of the acyl-CoA pool.

ACBP acts as a potent protector of acetyl-CoA carboxylase and mitochondrial adenine nucleotide translocase against inhibition by long chain acyl-CoA esters. It has also been shown to protect acyl-CoA against hydrolysis by microsomal hydrolases [4]. ACBP is able to transport and donate acyl-CoA to mitochondria for β-oxidation and to microsomes for glycerolipid synthesis. ACBP also stimulates the mitochondrial long chain acyl-CoA synthetase [5]. Long-chain acyl-CoA esters are an intermediate in lipid metabolism and modulate a wide range of cellular functions, such as energy metabolism regulation, lipid synthesis, signal transduction, ion flow regulation and gene expression [5].

Multiple ACBP isoforms have been observed in the majority of eukaryotic phyla examined, with the exception of fungal phyla [3,6], and it has been suggested that different ACBP isoforms have distinct properties and differing abilities to perform specific functions [2]. The broad range of ACBP distribution throughout the eukaryotes and its high degree of similarity across different tissues and species indicate that ACBP is a pivotal player in the trafficking and use of long chain acyl-CoA esters [2]. ACBP is a essential protein [7] whose function is associated with one or more basic function(s) common to all cells. Disruption of ACBP expression via RNAi renders HepG2, HeLa and Chang cells unable to grow in culture [8], and homologous recombination experiments have shown that ACBP is required for the viability of *Trypanosoma brucei* [9]. Depletion of ACBP in *Saccharomyces cerevisiae* results in severe growth retardation and changes in vacuoles and the plasma membrane [10,11], affects vesicular trafficking, organelle biogenesis and membrane assembly, reduces both the levels of very-long-chain fatty acids (C_{26}) and sphingolipid synthesis [11], and affects ceramide levels and protein trafficking [10]. All of the above data suggest that ACBP is a critical protein.

* Corresponding author. Tel.: +55 73 3680 5195; fax +55 73 3680 5228.
E-mail address: cascardo@uesc.br (J.C.M. Cascardo).

1570-9639/$ – see front matter
doi:10.1016/j.bbapap.2009.09.020

Crystal structures of ACBP from *Plasmodium falciparum* [12], cow [12,13], yeast [14], armadillo [15] and human [16] were deposited in the Protein Data Bank (PDB) and classified as four-helix bundles with an up-down-down-up bundle topology with an overhand loop connecting helices 2 and 3. The bundle arrangement of ACBP is unique among proteins with known four-helix folds [6]. In the present study, the *acbp* gene from *M. perniciosa* was cloned, the protein was characterized, and its structure was resolved. This is the first structure that has been solved in this organism.

2. Materials and methods

2.1. Construction of expression vector

The sequence of the gene encoding ACBP was obtained from cDNA library sequencing of the *M. perniciosa* fruiting body [17] and analysis of contigs from the *M. perniciosa* genome project [18] (www.lge.ibi.unicamp.br/vassoura) using BLAST [19] and CLUSTALW [20].

First-strand cDNA isolated from a fruiting body was used as a template. A forward primer was designed to include an *Nde*I restriction site (5′-GGG G**CA TAT G**TC CAA AGC AAAG-3′), and the reverse primer was designed to include an *Eco*RI site (5′-GGG G**GA ATT C**TT AGG CAG CTT CAA TC-3′). PCR was performed using *Pfu* DNA polymerase (Promega) according to the manufacturer's instructions, with the following cycling parameters: 5 min denaturation at 95 °C, 35 cycles of 30 s at 95 °C, 30 s at 50 °C, 1 min at 72 °C, and a final 10 min elongation at 72 °C. Amplification products of about 330 bp were recovered on a 1% agarose gel. The pT7-blue3 and pET-28a plasmids (Novagen) were purified by mini-preparation from *Escherichia coli* DH5α transformants. Plasmid pT7-blue3 was digested by *Eco*RV, and pET-28a was digested by *Nde*I and *Eco*RI. The pT7-blue3 and *acbp* gene were ligated with T4 DNA ligase (New England BioLabs) at 4 °C overnight and transformed into *E. coli* DH5α. Transformants were selected on the chromogenic substrate X-gal. The *acbp* gene was then digested with *Nde*I and *Eco*RI and recovered on a 1% agarose gel. The pET-28a-*acbp* construct was synthesized by treating with T4 DNA ligase for 2 hours at ambient temperature; *E. coli* DH5α cells transformed with this plasmid were selected on LB agar plates containing kanamycin (50 mg / mL). The pET-28a-*acbp* product obtained from *E. coli* transformants was confirmed by PCR and restriction mapping and used to transform *E. coli* BL21 (DE3). The *acbp* gene sequence of pET-28a-*acbp* was confirmed by sequencing, which involved 25 cycles of PCR amplification of 10 μL reaction volumes containing about 200 ng plasmid DNA, 10 pmol/μL each of primers T7 promoter and T7 terminator (Novagen), and 4 μL ET Dye Terminator (GE Healthcare). Sequencing reactions were ethanol precipitated, pellets were resuspended in 3.5 μL of loading buffer, 1.5 μL was loaded onto a sequencing gel, and data were collected by an ABI PRISM 377 DNA Sequencer (Perkin Elmer; Applied Biosystems).

2.2. ACBP purification

The pre-culture was grown overnight at 37 °C with agitation, inoculated at a ratio of 1:100, and grown in culture to an OD_{600} of 0.6. Expression was induced by the addition of 0.5 mM IPTG and allowed to proceed for 4 h at 37 °C. The cells were centrifuged at 5000×*g* for 15 min at 4 °C and then suspended in 50 mM sodium phosphate (pH 7.0) buffer plus 300 mM NaCl and 20 mM imidazole. The cells were lysed with a 7-min sonication and centrifuged at 20,000×*g* for 20 min at 4 °C, and the ACBP in the soluble fraction was purified with a TALON polyhistidine-tag purification resin (Clontech). The column was equilibrated with 10 column volumes, washed with 30 column volumes and eluted with 6 column volumes of buffer containing 200 mM imidazole. The histidine tail was removed with bovine thrombin (Sigma) in 50 mM sodium phosphate at pH 7.2 and 100 mM NaCl. A second purification step was carried out with size-exclusion chromatography with a Superdex 75 HR10/30 using the AKTA Purifier FPLC System (GE/Amersham Pharmacia Biotech, Sweden) in 20 mM Tris at pH 7.2 and 150 mM NaCl. The oligomeric state of the fractions was evaluated by comparison to the retention volume of a standard sample of known molecular weight. The ACBP purification yielded protein of over 95% purity based on 15% SDS PAGE. The size-exclusion chromatography showed that the majority of protein was in monomeric form and another fraction was in dimeric form. The purified protein was concentrated to about 6 mg / mL using an Amicon Ultra centrifugal filter (Millipore) in 20 mM Tris at pH 7.0. Protein concentration was determined by the Bradford method [21].

2.3. Assays to determine affinity for acyl-CoA esters and oligomeric state

A test for ACBP affinity for acyl-CoA esters was performed using isoelectric focusing and isothermal titration calorimetry (ITC). The oligomeric states of the apoprotein and the bound protein were evaluated by fluorescence anisotropy, dynamic light scattering (DLS) and native polyacrylamide gel electrophoresis (Native PAGE). Lauroyl-CoA (C12:0), myristoyl-CoA (C14:0), palmitoyl-CoA (C16:0), stearoyl-CoA (C18:0) and arachidoyl-CoA (C20:0) from Sigma were used as ligands in these experiments.

2.3.1. Isoelectric focusing

The pI of the ACBP at 80 μM in the apo and liganded form with ten-fold excess ligand was determined in an isoelectric focusing gel with a pH range of 3–9 (PhastGel™ IEF 3–9, GE Healthcare Life Sciences, Sweden), using the Pharmacia Phast System (GE Healthcare Life Sciences, Sweden) according to the manufacturer's protocols. The Broad pI kit pH 3–10 (GE Healthcare Life Sciences, Sweden) was used as a pI marker. The gel was stained with Coomassie Blue.

2.3.2. Isothermal titration calorimetry

All microcalorimetry experiments were carried out in 20 mM Tris, pH 7.0 at 25 °C, using approximately 11- to 18-fold excess ligand. The monomeric protein solution (13 to 18 μM) was placed in the calorimeter cell with a volume of 1.4173 mL and stirred at 300 rpm. All solutions were thoroughly degassed by stirring under vacuum before use. The sample was titrated with 200–260 μM ligand solution, and the final ligand concentration was determined using a millimolar extinction coefficient of 15.4 at 254 nm. The proportion of ligand and proteins used were similar to those used in previous experiments [22–24]. In total, 30 ligand injections of 8 μL each were added into the calorimeter cell at 130-s intervals from a 300-μL stirring syringe. The reference cell was filled with the same buffer used in the binding assay. All experiments were replicated four times at different protein concentrations, and the best-fit isotherm was used for association constant analysis. Ligand binding to ACBP was analyzed in a VP-ITC microcalorimeter from Microcal Inc. (Northampton, MA). Thermogram data were integrated and fitted to a theoretical titration curve using the ORIGIN software supplied by Microcal Inc. The association constant was calculated with equations for two sets of independent sites:

$$K_1 = \Theta_1 / (1 - \Theta_1)[X] \quad (1)$$

$$K_2 = \Theta_2 / (1 - \Theta_2)[X] \quad (2)$$

where K_1, K_2, Θ and *[X]* are the first binding constant, second binding constant, fraction of sites occupied by ligand *X* and free concentration of ligand, respectively.

2.3.3. Fluorescence anisotropy

The mean rotational anisotropy of the fluorescent residues of the entire apoprotein and the bound protein were evaluated by fluorescence anisotropy in an ISS K2 Multifrequency Phase Fluorometer

(Champaign, IL) using a 280-nm excitation wavelength. Intrinsic polarized fluorescence anisotropy assay measurements were done using the samples from microcalorimetry analysis after ligand titration and for the monomeric form used as a reference in the ITC experiments. The dimeric form was obtained from the appropriate size-exclusion chromatography fraction and was used at the same concentration as the monomeric form. Measurements were made in 0.5 mL in a 1-cm path length quartz cuvette. Prior to analysis, the microcalorimetry samples were diluted 10-fold in 20 mM Tris at pH 7.0. Possible free ligand contributions were subtracted from all the protein-ligand sample measurements. The anisotropy was recorded as the mean of 10 measurements across the samples under each condition. All assays were carried out at 25 °C. Values of fluorescence anisotropy (r) were measured according to the equation

$$(r) = (I_v - I_h) / (I_v + 2I_h) \quad (3)$$

where I_v and I_h are the intensities of emission when the polarizers are oriented parallel or perpendicular to the direction of the excitation polarizer, respectively. Polarization measurement variations were less than ± 0.005 for each sample.

2.3.4. Dynamic light scattering

DLS was used to determine the hydrodynamic radius (R_H) of ACBP at 2.5 μM, in its apo and liganded form using six-fold excess ligand. The R_H is given by the Stokes–Einstein relation:

$$R_H = (K_B T) / (6\pi \eta D) \quad (4)$$

where k_B, T, η and D are the Boltzmann constant, absolute temperature in Kelvin, solvent viscosity and diffusion coefficient, respectively.

DLS measurements were carried out in an experimental buffer of 20 mM Tris at pH 7.0 using a Protein Solutions DynaPro 99 (Protein Solutions, Charlottesville, VA). The samples used were centrifuged at 16,000×g for 10 min before analysis. The assays were performed at 25 °C with an acquisition time of 2.5 s in a 12 μL cuvette. Thirty acquisitions were averaged in a single measurement, and three sequential measurements were performed for each sample of the apo and liganded form. Dynamics v.5.25.44 software (Protein Solutions Inc.) was used for the data collection and analysis.

2.3.5. Native polyacrylamide gel electrophoresis

Native PAGE analysis of 80 μM ACBP in the apo and liganded form, using ten-fold excess ligand, was performed according to the Laemmli method [25], with some modifications. The electrode buffer was adjusted to pH 8.3, 9.5 and 10. The pHs of the stacking and resolving gels were also changed to pH 9.5 and 10, respectively. The resolving gel contained 10% acrylamide. The stacking and resolving gels, electrode buffer, and gel-loading buffer were prepared without denaturing agents. The gel was stained with Coomassie Blue.

2.4. Crystallization and data collection

ACBP was concentrated to 6 mg/mL in 20 mM Tris pH 7.0 and crystallized by the hanging drop method, using 25% PEG-MME 550, 100 mM MES, pH 6.5, 10 mM $ZnSO_4$, and three-fold excess palmitoyl-CoA. The drops consisted of 1.5 μL of protein solution plus 1.5 μL of crystallization solution and were equilibrated against 500 μL of the crystallization solution. The crystals grew in about one week. Before dataset collection, the crystals were cryoprotected by soaking for about 30 s in mother liquor with 30% PEG-MME 550. X-ray diffraction data were collected at 100 K. Measurements were made in-house using a Rigaku ULTRAX18 generator using copper radiation ($\lambda = 1.5418$) and a Mar345dtb image plate, over 1° increments in φ for a total rotation of 360°. The data were indexed and integrated using the program MOSFLM [26] and scaled using the program SCALA from the CCP4 suite [27].

2.5. Structure solution and refinement

The structure of *M. perniciosa* ACBP was solved by employing molecular replacement (MR) using the Phaser program [28] and using human ACBP (52% identity) as a search model (PDB ID 2FJ9) [16]. The MR solution was used as an initial model for automatic model building using the ARP/wARP program [29].

Model refinement was carried out initially with REFMAC [30] and Phenix [31] employing TLS parameters in the last stages of refinement. The model-building was performed with COOT [32] using σ_a-weighted 2Fo-Fc and Fo-Fc electron density maps. A total of 265 water molecules were included by both COOT and Phenix, and the MES molecule and Zn^{2+} ion were added using COOT.

In all cases, the behavior of R_{free} was used as the principal criterion for validating the refinement protocol. The stereochemical quality of the model was evaluated with PROCHECK [33] and MolProbity [34]. The coordinates and structure factors have been deposited in the PDB as 3FP5. Complete statistics for data collection and refinement are summarized in Table 1.

3. Results and discussion

3.1. Gene sequence and ACBP isoforms

Analysis of the *acbp* gene from the *M. perniciosa* Genome Project [18] has identified two possible sequences for ACBP. One sequence represents the classical ACBP, encoding a protein with 90 amino acids (isoform 1) [35]. The second sequence represents an isoform with 104 amino acids, which is deposited in GenBank as EEB92840 (referred to in the present study as isoform 2). Various isoforms of ACBP have been found in different organisms, with the exception of fungi; four to six isoforms have been identified in nematode, arthropod and vertebrate species, while mammals have three tissue-specific isoforms [2]. Fig. 1 shows an alignment of *M. perniciosa* ACBP isoforms with human, bovine, yeast, *Theobroma cacao* (sequence not deposited), *Ricinus communis*, *Panax ginseng*, *Zea mays* and *Sorghum bicolor* ACBP sequences. Isoform 2 showed identities of 54% to human, 54% to cow, 47% to isoform 1, 43% to *T. cacao*, 42% to *R. communis*, 42% to *P.*

Table 1
Full data collection and refinement statistics.

Data processing	
Space group	$P2_12_12_1$
Unit cell parameters	
a, b, c (Å)	32.39, 40.96, 82.28
α, β, γ	90°, 90°, 90°
Redundancy	13.1 (12.4)
R_{meas} (%)	5.5 (36.80)
R_{sym} (%)	5.1 (36.8)
Completeness (%)	97.5 (84.1)
Total reflections	199449 (22624)
Unique reflections	14876 (1825)
$I/\sigma I$	34.8 (7.0)
Refinement parameters	
Resolution range (Å)	18.64–1.59 (1.68–1.59)
R_{work} (%)	18.64
R_{free} (%)	21.24
Contents of asymmetric unit	
Protein atoms	872
Water molecules	265
Ligand atoms	13
RMSD geometry	
Bond lengths (Å)	0.007
Bond angles (°)	0.926
Overall B-factor (Å^2)	18.6
Ramachandran plot	
Most favored (%)	94.7
Additional allowed (%)	5.3
Outliers (%)	0

The values in parentheses refer to statistics in the highest bin.

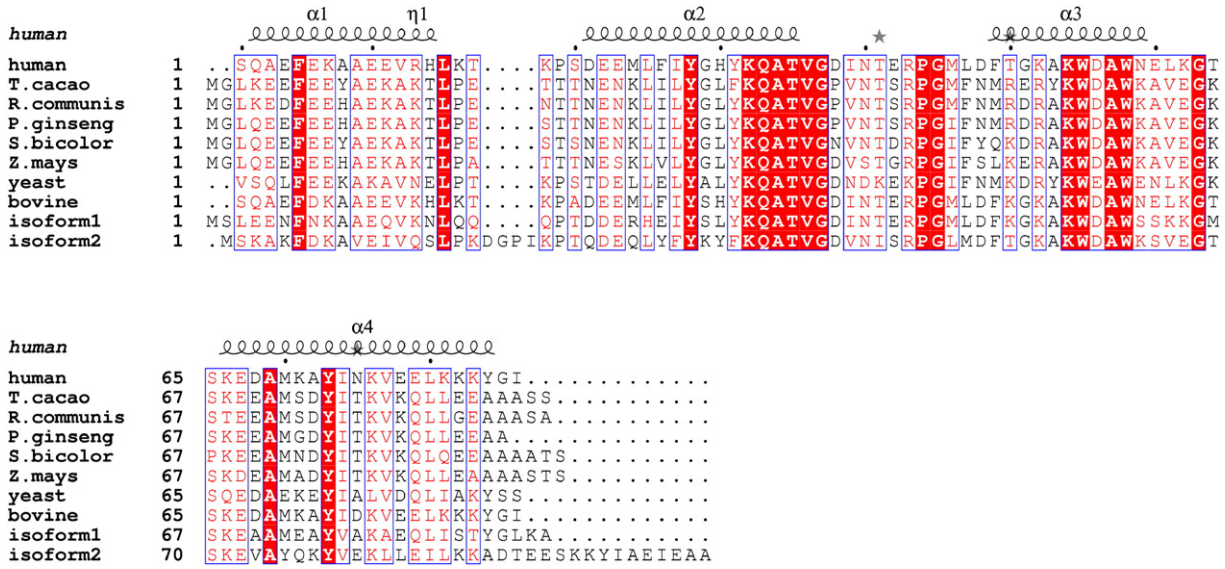

Fig. 1. Alignment of ACBP sequences. Alignment of ACBP isoforms 1 and 2 from *M. perniciosa* with human (PDB: 2FJ9), cow (PDB: 1HB6), yeast (PDB: 1ST7), *T. cacao* (sequence not deposited), *R. communis* (GenBank: CAA70200), *P. ginseng* (GenBank: BAB85987), *S. bicolor* (GenBank: EES14605) and *Z. mays* (GenBank: ACG27448) ACBP sequences.

ginseng, 40% to *Z. mays*, 38% to *S. bicolor*, and 34% to yeast variants when aligned with CLUSTALW. These results show that the *M. perniciosa* ACBPs are more closely related to the human L-ACBP than to the yeast ACBP. However, though this isoform of ACBP is exclusive to fungi, a BLAST search of non-redundant protein sequences showed greater percentage identity with basidiomycete ACBPs, which range from 104 to 110 amino acids in length. BLAST results showed the following percent identities with basidiomycota: *Coprinopsis cinerea* (XP_001836410), 74%; *Laccaria bicolor* (XP_001880619), 70%; *Cryptococcus neoformans* (XP_568458), 63%; *Ustilago maydis* (XP_759106), 61%; and *Malassezia globosa* (XP_001729358), 51%. The conserved residues observed in the alignment are involved in the interactions between α-helices 1 (Phe6), 2 (Thy33, Lys37, Gln38, Ala39, Thr40, Val41 and Gly42), 3 (Lys59, Trp60, Asp61, Ala62 and Trp63) and 4 (Ala74 and Tyr78); others residues have been changed but retained their key characteristics (similarity). These conserved residues are important for the maintenance of the characteristic folding of ACBP, and some are also involved in coenzyme A binding. The fact that ACBPs are highly conserved indicates that the search for species-specific ACBP inhibitors may be a difficult task.

3.2. Oligomeric state and binding studies

Analysis of size-exclusion chromatography data showed that about 80% of unliganded *M. perniciosa* ACBP exists in monomeric form, with the remaining 20% found as dimers (data not shown). Measurements of these fractions using fluorescence anisotropy and a dynamic light scattering technique for rotational diffusion and hydrodynamic radius (R_H), respectively, were compared with those from the monomeric fraction bound to various ligands (Fig. 2). The results suggested that *M. perniciosa* ACBP interacts with ligands and that the equilibrium shifts from the monomeric to the dimeric state principally when bound to long-chain acyl-CoA esters. These data are confirmed by native gel electrophoresis (Fig. 3B), which shows that liganded ACBP assumes dimeric states and preferentially binds long fatty chain acyl-CoA esters. In overview, DLS, anisotropy and native PAGE analysis indicate that monomeric *M. perniciosa* ACBP binds lauroyl-CoA and myristoyl-CoA preferentially, while the dimeric form binds more strongly to the other, larger acyl-CoA esters. Isoelectric focusing gel analysis (Fig. 3A) indicates that monomeric ACBP and ACBP in the presence of lauroyl-CoA present the same pI (~8.2), while

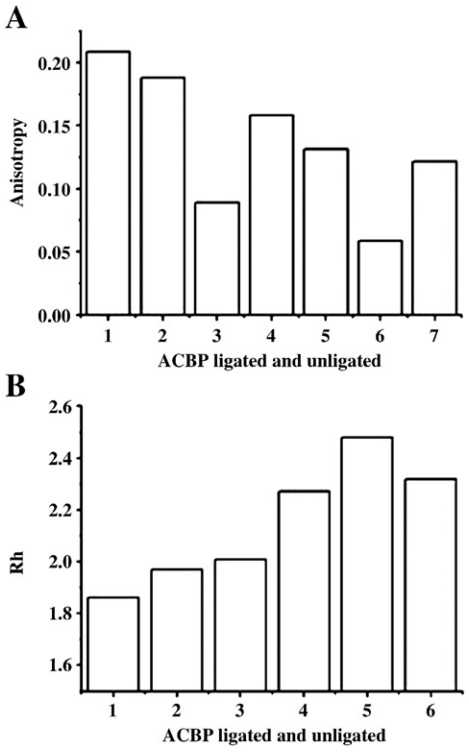

Fig. 2. Oligomeric states of ACBP. (A) The mean rotational diffusions of the entire apoprotein and the bound protein were evaluated by fluorescence anisotropy using the samples from microcalorimetry analysis after ligand titration compared with monomer and dimer forms. (1) Monomeric ACBP. (2) ACBP-lauroyl-CoA. (3) ACBP-myristoyl-CoA. (4) ACBP-palmitoyl-CoA. (5) ACBP-stearoyl-CoA. (6) ACBP-arachidoyl-CoA. (7) ACBP dimer. The rotational diffusion of the bound proteins incline to the dimer form, principally in the presence of larger (longer chain) ligands. (B) Dynamic light scattering measurement of hydrodynamic radius (R_H). (1) The monomer form of ACBP, with a calculated M_r of 14.4 kDa. (2(ACBP-Lauroyl-CoA (M_r 15.5 kDa). (3) ACBP-myristoyl-CoA (M_r 17.2 kDa). (4) ACBP-palmitoyl-CoA (M_r 23 kDa). (5) ACBP-stearoyl-CoA (M_r 28.2 kDa). (6) ACBP-arachidoyl-CoA (M_r 24.1 kDa). ACBP bound to palmitoyl-CoA, stearoyl-CoA or arachidoyl-CoA assumes a dimeric form in the presence of ligand, while ACBP bound to lauroyl-CoA and myristoyl-CoA assumes intermediate values for R_H, suggesting a mix of monomeric and dimeric forms.

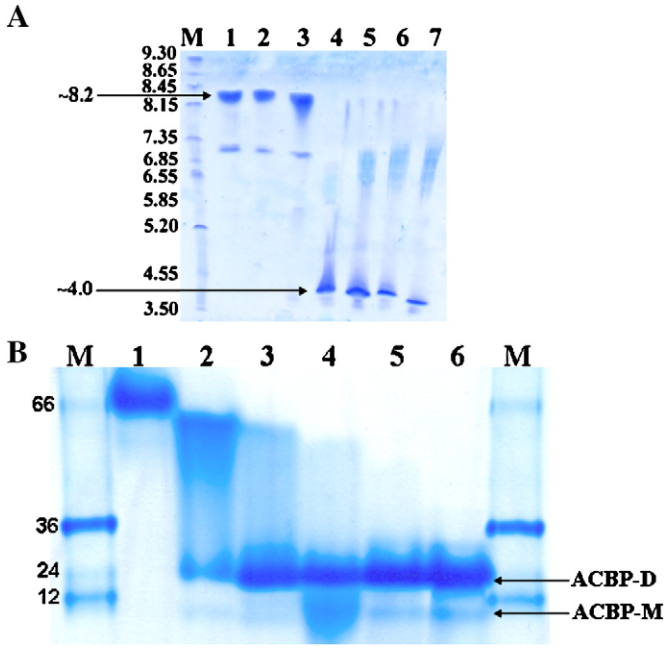

Fig. 3. Assays of binding and oligomeric states. (A) Isoelectric focusing gel. M—Marker showing pI. (1) Monomer ACBP. (2) ACBP-lauroyl-CoA. (3) ACBP-myristoyl-CoA. (4) ACBP-palmitoyl-CoA. (5) ACBP-stearoyl-CoA. (6) arachidoyl-CoA. A pI of about 8.2 is observed for monomer ACBP and ACBP-lauroyl-CoA, while a pI of about 4 is found for ACBP bound to ligands with chains of 14 to 20 carbons, suggesting that *M. perniciosa* ACBP has higher affinity for long chain acyl-CoA. (B) 10% Native PAGE. M—Marker showing M_r. (1) Monomeric ACBP. (2) ACBP-lauroyl-CoA. (3) ACBP-myristoyl-CoA. (4) ACBP-palmitoyl-CoA. (5) ACBP-stearoyl-CoA. (6) ACBP-arachidoyl-CoA. ACBP assumes a dimeric form (ACBP-D) primarily when it is bound to long chain acyl-CoAs. A fraction remaining in the monomeric state (ACBP-M) can be seen. ACBP monomers and ACBP incubated with smaller acyl-CoA esters do not assume correct sizes due to pI (~8.2), and do not separate in native PAGE.

a pI shift (to ~4) is observed when the protein is liganded with myristoyl-CoA, palmitoyl-CoA, stearoyl-CoA and arachidoyl-CoA, suggesting that binding occurs [23]. Binding data are in accordance with measurements proposed by other authors, where acyl-CoA esters with acyl chains between 14 and 22 carbon atoms in length are favored at the binding site [36]. The monomeric version of ACBP has a pI of around 8.2. This property prevents the measurement of accurate molecular mass by native PAGE, since the buffer used has a pH of 8.3 (at this pH, ACBP charge is near zero; therefore, it did not resolve well in the gel, generating a stain instead of a clear band). The use of the buffer at pH 9.5 and 10, well as in the stacking and resolving gels in the same pH, shows small differences in the run of the monomeric ACBP in the apo form (data not shown). These results may be due to the low charge of the ACBP at these pHs. Thus, the switch from monomer to dimer observed by DLS and fluorescence anisotropy cannot be shown by native PAGE. However, equilibrium between monomeric and dimeric forms bound to acyl-CoA esters can be observed in this assay, with the dimer state predominating (Fig. 3B).

ITC data obtained from *M. perniciosa* ACBP (Table 2) shows differential isotherms as compared to other studied ACBPs (Fig. 4), which is likely the reason that *M. perniciosa* ACBP preferentially enters a dimeric state when it is liganded. Isotherms of *M. perniciosa* ACBP are fitted for two sites (or two sequential binding sites) for lauroyl-CoA, myristoyl-CoA and palmitoyl-CoA, while other ACBPs bound in monomeric form are fitted to one site [22–24,37]. The two-site model was assumed to be the simpler model, and all ligands cannot be fitted as sequential binding sites. However, the real model must be more elaborate, due to the fact that the first ligand must be bound in order to induce dimerization, or dimerization must occur concomitant with binding so that the second ligand can be bound. In the analysis presented in Table 2, the association constants do not clearly show whether there are two binding sites on a single ACBP molecule or whether the two sites are due to dimer formation. The ACBP structures deposited in the PDB and the analysis of the *M. perniciosa* ACBP structure indicate that it is almost impossible for two ligands to be bound in the monomeric structure. The monomeric structure presents only one binding site for coenzyme A, and the ligand involves a significant portion of the protein. Therefore, two sites must be formed through of the dimerization, as was observed in the human ACBP structure, where two ligands are bound to dimers [16]. Consistent with this, experiments using tyrosine fluorescence quenching as an indication of acyl-CoA binding to bovine ACBP indicated a binding stoichiometry of 1 mol of acyl-CoA/2 mol of ACBP. This indicates that bovine ACBP appears as a dimer in solution or that ligand binding induces dimer formation [38]. Considering that *M. perniciosa* ACBP data can be fitted to a two-binding site model, we can assume that the first association constant is the main step of acyl-CoA ester binding. In this model, the association constant (K_1) increases when binding larger acyl-CoA esters, indicating that *M. perniciosa* ACBP binds preferentially to long-chain acyl-CoA esters (Table 2). The K_1 and K_2 for binding lauroyl-CoA have standard errors greater than the association constants themselves, probably because lauroyl-CoA has low affinity for ACBP, as observed in native PAGE and isoelectric focusing gel experiments (Fig. 3A). Moreover, the analysis of the DLS and anisotropy data indicates that *M. perniciosa* ACBP bound to lauroyl-CoA is more monomeric than dimeric. Interestingly, the ITC data for lauroyl-CoA-ACBP binding fit well to two-site or two sequential binding site models, but cannot fit a one-site model. The K_1 for lauroyl-CoA with ACBP is lower than that for other acyl-CoA esters; these data may explain why the liganded compound is not found by an isoelectric focusing gel and a native PAGE. However, if lauroyl-CoA can bind to ACBP, the second association constant is important in determining whether that event will occur, if it is greater than the first constant. The K_d values for *M. perniciosa* ACBP using K_1 from lauroyl-CoA (two sequential binding sites), myristoyl-CoA, palmitoyl-CoA, stearoyl-CoA and arachidoyl-CoA were approximately 109 nM, 57 nM, 55 nM, 2 nM and 0.65 nM, respectively. Comparison of these data with the K_d values from other organisms indicates that *M. perniciosa* ACBP has greater affinity for arachidoyl-CoA than *Trypanosoma cruzi* ACBP has for myristoyl-CoA (0.35 nM) [39] or than yeast ACBP has for palmitoyl-CoA (0.55 nM) [23]; these values are minor

Table 2
Association constants of ACBP-acyl-CoA ester binding.

Acyl-CoA	2 sites K_1 (M^{-1})	2 sites K_2 (M^{-1})	2 sequential sites K_1 (M^{-1})	2 sequential sites K_2 (M^{-1})
Lauroyl-CoA[a]	$(1.48 \pm 7.34) \times 10^4$	$(1.47 \pm 3.77) \times 10^7$	$(9.19 \pm 1.70) \times 10^6$	$(1.89 \pm 1.00) \times 10^3$
Myristoyl-CoA	$(1.75 \pm 0.88) \times 10^7$	$(1.46 \pm 1.40) \times 10^4$	$(1.54 \pm 0.27) \times 10^7$	$(1.45 \pm 0.27) \times 10^4$
Palmitoyl-CoA	$(1.85 \pm 1.42) \times 10^7$	$(8.60 \pm 7.30) \times 10^4$	$(7.69 \pm 1.30) \times 10^6$	$(1.21 \pm 0.86) \times 10^4$
Stearoyl-CoA	$(4.21 \pm 1.68) \times 10^8$	$(1.04 \pm 0.40) \times 10^6$	–	–
Arachidoyl-CoA	$(1.55 \pm 1.34) \times 10^9$	$(1.56 \pm 1.12) \times 10^6$	–	–

Parameters obtained from isotherms of ACBP-acyl-CoA ester binding. The standard errors were obtained with the ORIGIN program using the best fit of two binding sites and two sequential sites for one protein concentration of each ligand.

[a] Lauroyl-CoA has a standard error greater than K_1 (first association constant) and K_2 (second association constant) for two sites. Data for stearoyl-CoA and arachidoyl-CoA cannot be fitted in the two sequential binding sites model.

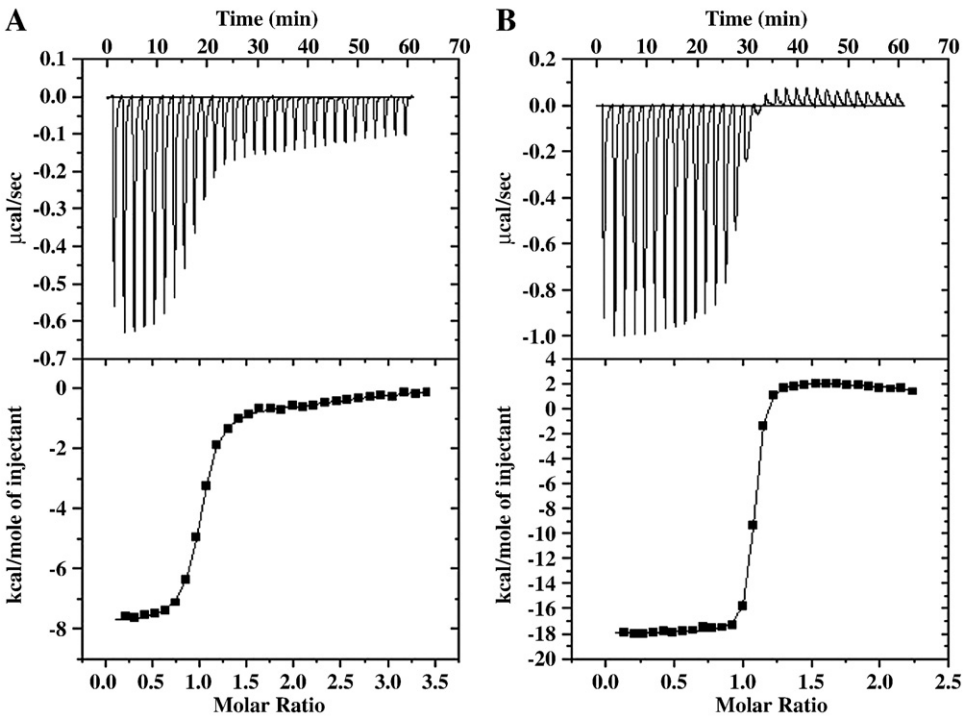

Fig. 4. Isotherms from binding ACBP-acyl-CoA. Isotherms from binding ACBP-acyl-CoA fitted with two sites. (A) ACBP-palmitoyl-CoA. (B) ACBP-arachidoyl-CoA.

compared to the affinity of bovine ACBP for palmitoyl-CoA (4.5 pM) [22]. The minor affinity found for lauroyl-CoA is similar to the K_d value of bovine ACBP and capryloyl-CoA (approximately 277 nM) [24]. These data are consistent with the low affinity for lauroyl-CoA obtained in the isoelectric focusing gel and native PAGE. The K_d values obtained for myristoyl-CoA and palmitoyl-CoA were similar to that found for armadillo ACBP, which has a range of 34 to 75 nM for palmitoyl-CoA [15]. The comparison indicates that *M. perniciosa* ACBP shows as high an affinity for long-chain acyl-CoA esters as does bovine ACBP, while *T. cruzi* ACBP has affinity for short-chain acyl-CoA esters, as previously reported [39]. This result suggests that the *M. perniciosa* ACBP has a greater affinity for long acyl-CoA esters with carbon chains up to C20. This can also be observed in the isothermal data we obtained, where the change from an exothermic to an endothermic isothermal was observed only with arachidoyl-CoA as a ligand, while this change is observed with minor acyl-CoA esters in ITC studies of bovine ACBP [24,37,22].

Analysis of acyl-CoA binding from isoelectric focusing gels and native PAGE showed that ACBP binds lauroyl-CoA weakly, but binds to other acyl-CoA esters with long acyl-CoA chains with greater affinity. The ITC data is in agreement with these data, where the lowest K_1 was observed for binding lauroyl-CoA, and increasing values of K_1 were observed when binding to longer acyl-CoA chains.

Other than human ACBP, all the proteins studied so far present as monomers in native form or when bound to acyl-CoA esters. The data obtained from DLS and native PAGE indicate that the *M. perniciosa* ACBP behaves as a monomer in its native form, but as a dimer when it is bound with acyl-CoA esters. The mutation of His to Ser in α-helix 1 (from human to *M. perniciosa* ACBP) may be responsible for the failure of *M. perniciosa* ACBP to adopt a hexameric state, as does human ACBP. However, bovine ACBP, which contains the same residues as human ACBP, does not form a dimer when bound to acyl-CoA ester. These differing states for the three bound ACBPs can be attributed to structural differences. The *M. perniciosa* ACBP has the longest loop I of all the ACBP structures. Since this loop in human ACBP interacts with the terminus of fatty acids, this is consistent with our finding that the *M. perniciosa* ACBP may preferentially bind acyl-CoA esters with long fatty acids chains up 20 carbons. (Fatty acid chains above 20 carbons were not used in this work.) In order for this to occur, the *M. perniciosa* ACBP must be in dimer form, whereas bovine ACBP can bind shorter fatty acid chains when in monomer form.

3.3. Moniliophthora perniciosa ACBP structure description

The three-dimensional structures of ACBP from cow [12,13,40], *P. falciparum* [12], yeast [14], armadillo [15] and human [16] have been solved. All structures present the fold of the peptide backbone as an up–down–down–up four-helix bundle, which is a unique arrangement among the known four-helix folds [6]. The server CATH [41] classifies the topology of ACBP as an acyl-CoA binding protein, and SCOP [42] classifies the ACBP fold as a core of three helices, in a closed up-and-down bundle with a left-handed twist.

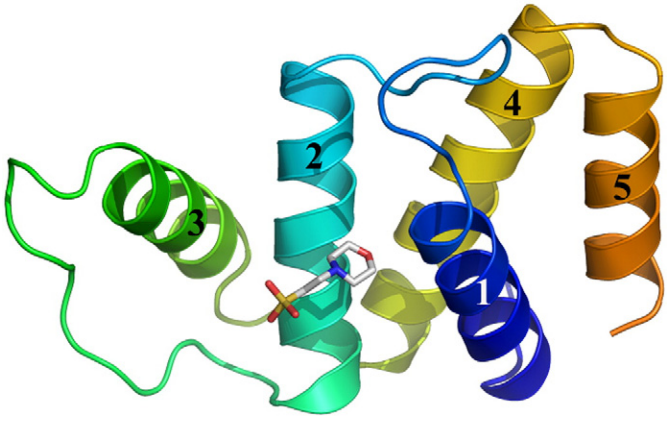

Fig. 5. The *M. perniciosa* ACBP structure. N-termini are shown in blue and C-termini are shown in orange, with an extra α-helix (5). The MES localized in the CoA binding site.

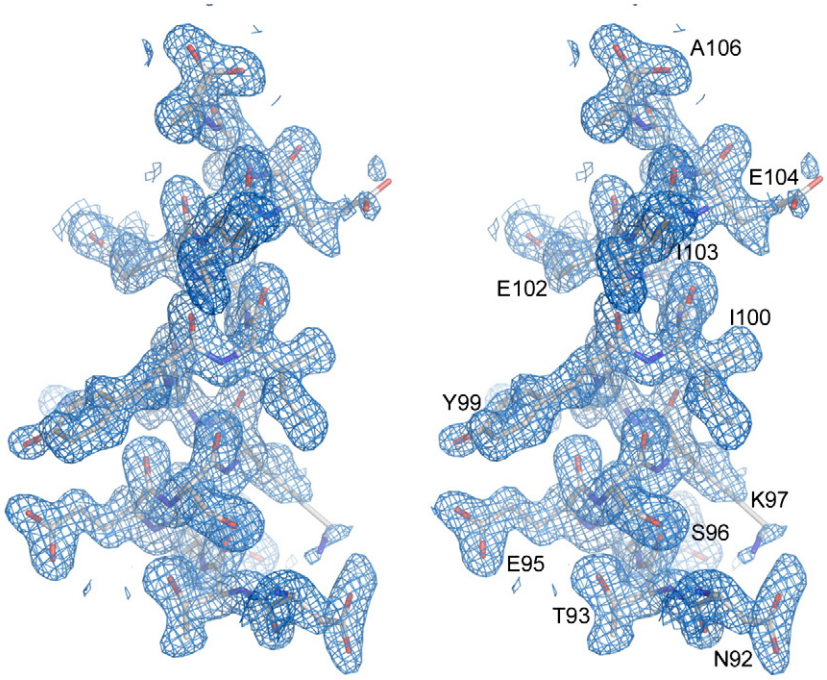

Fig. 6. Stereo image of the electron density map for the fifth α-helix. Stereo image of the electron density map 2Fo-Fc contoured at 1σ for the fifth α-helix in the *M. perniciosa* ACBP structure.

Neither described the ACBP fold as a classical four-helix bundle; indeed, the fourth helix has a packing angle of about 47° [43] while the classical definition of a four-helix bundle is restricted to structures containing acute interhelical angles no greater than 40°. From this point of view, the ACBP molecule could not be classified as a classical four-helix bundle.

The *M. perniciosa* ACBP structure presented here crystallizes in the orthorhombic space group $P2_12_12_1$, with one molecule per asymmetric unit. The *M. perniciosa* ACBP structure possesses 104 residues, plus two extra N-terminal residues resulting from his-tag cleavage of the original protein expressed from a pET28a construct. The structure of *M. perniciosa* is similar to that of other ACBPs. However, it contains an extra helix at its C-terminus for a total of five α-helices (helix 1—residues 3–15; helix 2—residues 26–40; helix 3—residues 54–64; helix 4—residues 71–89 and helix 5—residues 92–103). This fifth helix is unique to the *M. perniciosa* ACBP (Figs. 5–6). The packing of helix 5 with helices 1, 2 and 4 forms a classical four-helix bundle (Fig. 7). The packing angles of the helices [44] are shown in Table 3. The packing angle between helices 1 and 4 is 47.13°; as previously described this acute angle could not be considered a classical four-helix bundle. However, the bundle formed between helices 1, 2, 4 and 5 can be classified as a classical four-helix bundle of type D. The presence of the fifth helix in *M. perniciosa* ACBP shows how a packing of five helices could form two distinct four-helix bundles in the same protein. Studies of molecule stability and of the structure of *M. perniciosa* bound to acyl-CoA esters may produce additional information about the function of the fifth α-helix.

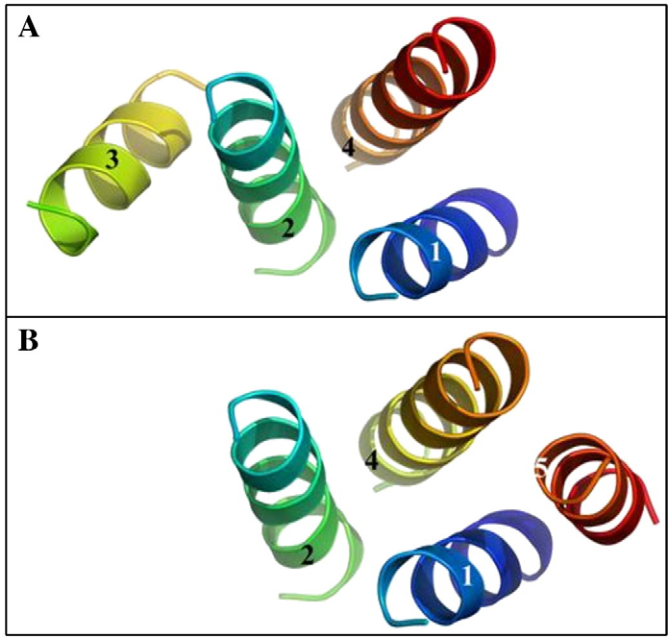

Fig. 7. Packing of the α-helices in *M. perniciosa* ACBP. (A) The typical topology of ACBP is an arrangement unique among known four-helix folds, formed by helices 1, 2, 3 and 4. (B) A classical four-helix bundle including helices 1, 2, 3 and 5. Panels A and B were made in the same orientation.

Loop I, located between α-helices 1 and 2, is larger (10 residues) than other ACBP loop structures (5 to 7 residues) (Fig. 1). The structure of the *M. perniciosa* ACBP contains two additional residues in the N-terminal region (Ser and His) as a result of the his-tag cleavage of the original protein expressed from a pET28a construct. The additional His participates in an ion–zinc interaction, together with Glu72 and Glu100 of the neighboring molecule. In bovine and human ACBP structures, cadmium [12] and zinc [16] ions are found coordinated by

Table 3
Helix-packing pairs.

Helix packing pair	Global angle	Local angle	Distance (Å)	Covalent	Electro	H-bond	VDW
1–2	−139.780	−138.505	12.044	0	0	0	1
2–3	−60.991	−60.704	8.060	0	0	1	6
1–4	47.133	46.334	9.012	0	0	0	4
2–4	−151.343	−150.835	7.184	0	1	0	7
4–5	−152.654	−150.310	6.074	0	0	1	2

The table shows packing angles and ligations and interactions found between these helices.

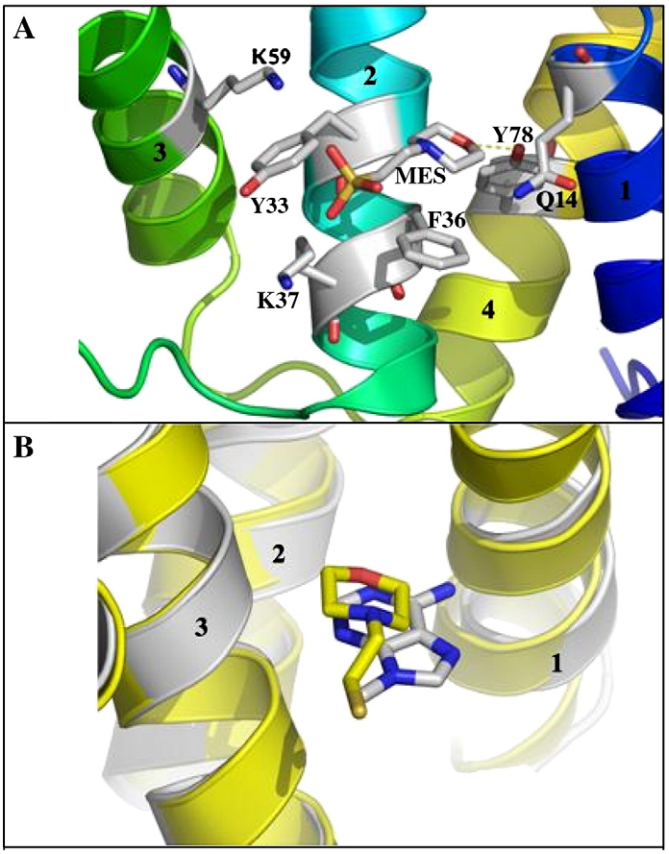

Fig. 8. MES bound to *M. perniciosa* ACBP. (A) Residues involved in MES binding to ACBP. (B) MES without a phosphate group is bound in the same location as the adenine from CoA, shown by superposition with the liganded human ACBP (2CB8).

His14 (on α-helix 1) and Glu11 and His15 (on α-helix 1), respectively. The His residue in α-helix 1 is found only in bovine and human ACBP structures, and these are the only structures that have ions bound. Therefore, this residue has an important function in binding ions, and when bound to Zn^{2+}, it is responsible for forming the human ACBP-myristoyl-CoA hexamer [16]. However, in the bovine structure, the metal ion is not involved in cluster formation, and this structure is found as a monomer in both the unbound and bound forms. In the *M. perniciosa* ACBP, the His residue is mutated to a Ser residue, and it is not possible to identify in the electron density map corresponding to the zinc ion. The bound zinc is localized at the additional His, which is not found in nature. Like the *M. perniciosa* ACBP, the *P. falciparum* structure [12] presents an additional His residue at the N-terminus and was found with a nickel ion bound (1HBK).

The binding of molecules from crystallization or even cryoprotection solutions is commonly observed in protein structures. A molecule of the MES used as a buffer in crystallization was found in the *M. perniciosa* ACBP structure, localized between α-helices 1 and 2 (Fig. 8A). The morpholine ring is piled atop Phe36 on α-helix 2, and the oxygen atom of the ring forms a hydrogen bond with Tyr78 on α-helix 4. The oxygen atoms from the ethanesulfonic group form van der Waals interactions with Gln14 (on α-helix 1), Tyr33, Lys37 (on α-helix 2) and Lys59 (on α-helix 3). The MES molecule is localized in the same orientation as the base adenine from coenzyme-A (Fig. 8B). In order to obtain MES-free crystals, the MES was exchanged for Bis-Tris in crystallization assays in the presence of ligands, but crystals could not be obtained.

ACBP has been identified as a housekeeping protein [7] and was proposed to play a pivotal role in the trafficking and use of long chain acyl-CoA esters [2]. ACBP was confirmed as an essential protein in different cell types [8] and in *T. brucei* [9]. Moreover, its depletion in *S. cerevisiae* causes severe alterations in growth, cell structure and metabolism [10,11]. ACBP validation studies in fungi are necessary to confirm whether this protein is essential for these organisms and thus whether ACBP might be a good target for new fungicide molecules. Interestingly, *M. perniciosa* ACBP bound MES in the traditional binding site of the adenine derived from CoA, suggesting that this region can be utilized in screening for small molecule inhibitors. The search for small molecules able to inhibit the binding between ACBP and acyl-CoA esters will be an important step toward obtaining drugs that repress acyl-CoA ester transport and consequently silence the function of this important protein in fungal pests. Initial candidates might be analogs of purines and pyrimidines.

Acknowledgements

The authors would like to thank Dr. Susana Andrea Sculaccio and Msc. Andressa Patricia Alves Pinto for technical assistance in gene sequencing, isoelectric focusing and isothermal titration calorimetry, and Dr. Leandro Seiji Goto for helpful in the fluorescence anisotropy analysis. P S Monzani was the recipient of a FAPESB postdoctoral fellowship. This work was supported by the *M. perniciosa* proteomic project. FINEP (Grant 01.07.0074-00) and FAPESB (Grant 1431080017116).

References

[1] M.P. McQuilken, Supriadi, S.A. Rudgard, Sensitivity of *Crinipellis perniciosa* to two triazole fungicides in vitro and their effect on development of the fungus in cocoa, Plant Pathol. 37 (1988) 499–506.
[2] N.J. Faergeman, M. Wadum, S. Feddersen, M. Burton, B.B. Kragelund, J. Knudsen, Acyl-CoA binding proteins; structural and functional conservation over 2000 MYA, Mol. Cell Biochem. 299 (2007) 55–65.
[3] J. Knudsen, BurtonM. , FaergemanN,J , Long-chain acyl-CoA esters and acyl-CoA binding protein (ACBP) in cell function, in: G.v.d. Vusse (Ed.), Lipobiology, Elsevier, Amsterdam, 2004, pp. 123–152.
[4] J.T. Rasmussen, J. Rosendal, J. Knudsen, Interaction of acyl-CoA-binding protein (ACBP) on processes for which acyl-CoA is a substrate, product or inhibitor, Biochem. J. 292 (1993) 907–913.
[5] N.J. Faergeman, J. Knudsen, Role of long-chain fatty acyl-CoA esters in the regulation of metabolism and in cell signalling, Biochem. J. 323 (1997) 1–12.
[6] B.B. Kragelund, J. Knudsen, F.M. Poulsen, Acyl- coenzyme A binding protein (ACBP), BBA Mol. Cell Biol. Lipids 1441 (1999) 150–161.
[7] S. Mandrup, R. Hummel, S. Ravn, G. Jensen, P.H. Andreasen, N. Gregersen, J. Knudsen, K. Kristiansen, Acyl-Coa-binding protein/diazepam-binding inhibitor gene and pseudogenes. A typical housekeeping gene family, J. Mol. Biol. 228 (1992) 1011–1022.
[8] N.J. Faergeman, J. Knudsen, Acyl-CoA binding protein is an essential protein in mammalian cell lines, Biochem. J. 368 (2002) 679–682.
[9] K.G. Milne, M.L.S. Güther, M.A.J. Ferguson, Acyl-CoA binding protein is essential in bloodstream form *Trypanosoma brucei*, Mol. Biochem. Parasitol. 112 (2001) 301–304.
[10] N.J. Faergeman, S. Feddersen, J.K. Christiansen, M.K. Larsen, R. Schneiter, C. Ungermann, K. Mutenda, P. Roepstorff, J. Knudsen, Acyl-CoA-binding protein, Acb1p, is required for normal vacuole function and ceramide synthesis in *Saccharomyces cerevisiae*, Biochem. J. 380 (2004) 907–918.
[11] B. Gaigg, T.B.F. Neergaard, R. Schneiter, J.K. Hansen, N.J. Faergeman, N.A. Jensen, J. R. Andersen, J. Friis, R. Sandhoff, H.D. Schroder, J. Knudsen, Depletion of acyl-coenzyme A-binding protein affects sphingolipid synthesis and causes vesicle accumulation and membrane defects in *Saccharomyces cerevisiae*, Mol. Biol. Cell 12 (2001) 1147–1160.
[12] D.M.F. van Aalten, K.G. Milne, J.Y. Zou, G.J. Kleywegt, T. Bergfors, M.A.J. Ferguson, J. Knudsen, T.A. Jones, Binding site differences revealed by crystal structures of *Plasmodium falciparum* and bovine acyl-CoA binding protein, J. Mol. Biol. 309 (2001) 181–192.
[13] K.V. Andersen, F.M. Poulsen, The three-dimensional structure of acyl-coenzyme A binding-protein from bovine liver: structural refinement using heteronuclear multidimensional NMR spectroscopy, J. Biomol. NMR 3 (1993) 271–284.
[14] K. Teilum, T. Thormann, N.R. Caterer, H.I. Poulsen, P.H. Jensen, J. Knudsen, B.B. Kragelund, F.M. Poulsen, Different secondary structure elements as scaffolds for protein folding transition states of two homologous four-helix bundles, Proteins 59 (2005) 80–90.
[15] M.D. Costabel, M.R. Ermacora, J.A. Santome, P.M. Alzari, D.M.A. Guerin, Structure of armadillo ACBP: a new member of the acyl-CoA-binding protein family, Acta Crystallogr. F 62 (2006) 958–961.
[16] J.P. Taskinen, D.M. van Aalten, J. Knudsen, R.K. Wierenga, High resolution crystal structures of unliganded and liganded human liver ACBP reveal a new mode of binding for the acyl-CoA ligand, Proteins 66 (2007) 229–238.
[17] A.B.L. Pires, K.P. Gramacho, D.C. Silva, A. Goes-Neto, M.M. Silva, J.S. Muniz-Sobrinho, R.F. Porto, C. Villela-Dias, M. Brendel, J.C.M. Cascardo, G.A. Gonçalo, Early

development of *Moniliophthora perniciosa* basidiomata and developmentally regulated genes, BMC Microbiol. (Online) 9 (2009) 158.
[18] J.M.C. Mondego, M.F. Carazzole, G.G.L. Costa, E.F. Formighieri, L.P. Parizzi, J. Rincones, C. Cotomacci, D.M. Carraro, A.F. Cunha, H. Carrer, R.O. Vidal, R.C. Estrela, O. Garcia, D.P.T. Thomazella, B.V. de Oliveira, A.B.L. Pires, M.C.S. Rio, M.R.R. Araujo, M.H. de Moraes, L.A.B. Castro, K.P. Gramacho, M.S. Gonçalves, J.P. Moura Neto, A. Goes Neto, L.V. Barbosa, M.J. Guiltinan, B.A. Bailey, L.W. Meinhardt, J.C.M. Cascardo, A.G. Gonçalo, A genome survey of *Moniliophthora perniciosa* gives new insights into witches' broom disease of cacao, BMC Genomics 9 (2008) 548.
[19] S.F. Altschul, T.L. Madden, A.A. Schaffer, J.H. Zhang, Z. Zhang, W. Miller, D.J. Lipman, Gapped BLAST and PSI-BLAST: a new generation of protein database search programs, Nucleic Acids Res. 25 (1997) 3389–3402.
[20] J.D. Thompson, D.G. Higgins, T.J. Gibson, Clustal-W—improving the sensitivity of progressive multiple sequence alignment through sequence weighting, position-specific gap penalties and weight matrix choice, Nucleic Acids Res. 22 (1994) 4673–4680.
[21] M.M. Bradford, A rapid and sensitive method for the quantitation of microgram quantities of protein utilizing the principle of protein-dye binding, Anal. Biochem. 72 (1976) 248–254.
[22] J.T. Rasmussen, N.J. Faergeman, K. Kristiansen, J. Knudsen, Acyl-CoA-binding protein (ACBP) can mediate intermembrane acyl-CoA transport and donate acyl-CoA for β-oxidation and glycerolipid synthesis, Biochem. J. 299 (1994) 165–170.
[23] J. Knudsen, N.J. Faergeman, H. Skott, R. Hummel, C. Borsting, T.M. Rose, J.S. Andersen, P. Hojrup, P. Roepstorff, K. Kristiansen, Yeast acyl-CoA-binding protein: acyl-CoA-binding affinity and effect on intracellular acyl-CoA pool size, Biochem. J. 302 (1994) 479–485.
[24] N.J. Faergeman, B.W. Sigurskjold, B.B. Kragelund, K.V. Andersen, J. Knudsen, Thermodynamics of ligand binding to acyl-coenzyme a binding protein studied by titration calorimetry, Biochemistry 35 (1996) 14118–14126.
[25] U.K. Laemmli, Cleavage of structural proteins during the assembly of the head of bacteriophage T4, Nature 227 (1970) 680–685.
[26] A.G.W. Leslie, H.R. Powell, Processing diffraction data with MOSFLM, in: R.J. Read, J.L. Sussmann (Eds.), Evolving Methods for Macromolecular Crystallography, 245, Springer, Berlin, 2007, pp. 41–51.
[27] The CCP4 suite: programs for protein crystallography, Acta Crystallogr. D 50 (1994) 760–763.
[28] A.J. Mccoy, R.W. Grosse-Kunstleve, P.D. Adams, M.D. Winn, L.C. Storoni, R.J. Read, Phaser crystallographic software, J. Appl. Crystallogr. 40 (2007) 658–674.
[29] S.X. Cohen, M. Ben Jelloul, F. Long, A. Vagin, P. Knipscheer, J. Lebbink, T.K. Sixma, V. S. Lamzin, G.N. Murshudov, A. Perrakis, ARP/wARP and molecular replacement: the next generation, Acta Crystallogr. D 64 (2008) 49–60.
[30] G.N. Murshudov, A.A. Vagin, E.J. Dodson, Refinement of macromolecular structures by the maximum-likelihood method, Acta Crystallogr. D 53 (1997) 240–255.
[31] P.D. Adams, R.W. Grosse-Kunstleve, L.W. Hung, T.R. Ioerger, A.J. McCoy, N.W. Moriarty, R.J. Read, J.C. Sacchettini, N.K. Sauter, T.C. Terwilliger, PHENIX: building new software for automated crystallographic structure determination, Acta Crystallogr. D 58 (2002) 1948–1954.
[32] P. Emsley, K. Cowtan, Coot: model-building tools for molecular graphics, Acta Crystallogr. D 60 (2004) 2126–2132.
[33] R.A. Laskowski, M.W. MacArthur, D.S. Moss, J.M. Thornton, PROCHECK: a program to check the stereochemical quality of protein structures, J. Appl. Crystallogr. 26 (1993) 283–291.
[34] I.W. Davis, L.W. Murray, J.S. Richardson, D.C. Richardson, MOLPROBITY: structure validation and all-atom contact analysis for nucleic acids and their complexes, Nucleic Acids Res. 32 (2004) W615–619.
[35] J. Rincones, L.M. Scarpari, M.F. Carazzolle, J.M. Mondego, E.F. Formighieri, J.G. Barau, G.G. Costa, D.M. Carraro, H.P. Brentani, L.A. Vilas-Boas, B.V. de Oliveira, M. Sabha, R. Dias, J.M. Cascardo, R.A. Azevedo, L.W. Meinhardt, G.A. Pereira, Differential gene expression between the biotrophic-like and saprotrophic mycelia of the witches' broom pathogen *Moniliophthora perniciosa*, Mol. Plant Microbe Interact. 21 (2008) 891–908.
[36] J. Rosendal, P. Ertbjerg, J. Knudsen, Characterization of ligand binding to acyl-CoA-binding protein, Biochem. J. 290 (1993) 321–326.
[37] K.A.H. Abo-Hashema, M.H. Cake, M.A. Lukas, J. Knudsen, The interaction of acyl-CoA with acyl-CoA binding protein and carnitine palmitoyltransferase I, Int. J. Biochem. Cell Biol. 33 (2001) 807–815.
[38] J. Mikkelsen, J. Knudsen, Acyl-CoA-binding protein from cow. Binding characteristics and cellular and tissue distribution, Biochem. J. 248 (1987) 709–714.
[39] K.G. Milne, M.A.J. Ferguson, Cloning, expression, and characterization of the acyl-CoA-binding protein in African trypanosomes, J. Biol. Chem. 275 (2000) 12503–12508.
[40] B.B. Kragelund, K.V. Andersen, J.C. Madsen, J. Knudsen, F.M. Poulsen, Three-dimensional structure of the complex between acyl-coenzyme A binding-protein and palmitoyl-coenzyme A, J. Mol. Biol. 230 (1993) 1260–1277.
[41] L.H. Greene, T.E. Lewis, S. Addou, A. Cuff, T. Dallman, M. Dibley, O. Redfern, F. Pearl, R. Nambudiry, A. Reid, I. Sillitoe, C. Yeats, J.M. Thornton, C.A. Orengo, The CATH domain structure database: new protocols and classification levels give a more comprehensive resource for exploring evolution, Nucleic Acids Res. 35 (2007) D291–D297.
[42] A. Andreeva, D. Howorth, J.M. Chandonia, S.E. Brenner, T.J.P. Hubbard, C. Chothia, A.G. Murzin, Data growth and its impact on the SCOP database: new developments, Nucleic Acids Res. 36 (2008) D419–D425.
[43] S.R. Presnell, F.E. Cohen, Topological distribution of four-alpha-helix bundles, Proc. Natl. Acad. Sci. (1989) 6592–6596.
[44] J.A.R. Dalton, I. Michalopoulos, D.R. Westhead, Calculation of helix packing angles in protein structures, Bioinformatics 19 (2003) 1298–1299.